Classification of specimen density in Laser Powder Bed Fusion (L-PBF) using in-process structure-borne acoustic process emissions

N. Eschner*, L. Weiser, B. Häfner, G. Lanza

wbk – Institute of Production Science, Karlsruhe Institute of Technology, 76131 Karlsruhe, Germany

ABSTRACT

Currently, the laser powder bed fusion (L-PBF) process cannot offer a reproducible and predefined quality of the processed parts. Recent research on process monitoring focuses strongly on integrated optical measurement technology. Besides optical sensors, acoustic sensors also seem promising. Previous studies have shown the potential of analyzing structure-borne and air-borne acoustic emissions in laser welding. Only a few works evaluate the potential that lies in the usage during the L-PBF process.

This work shows how the approach to structure-borne acoustic process monitoring can be elaborated by correlating acoustic signals to statistical values indicating part quality. Density measurements according to Archimedes' principle are used to label the layer-based acoustic data and to measure the quality. The data set is then treated as a classification problem while investigating the applicability of existing artificial neural network algorithms to match acoustic data with density measurements. Furthermore, this work investigates the transferability of the approach to more complex specimens.

1. Introduction and structure of this article

The market segment of additive manufacturing (AM) is growing rapidly [1]. For manufacturing metal parts, the laser powder bed fusion (L-PBF) process is one of the most crucial manufacturing techniques [2]. One of the major drawbacks slowing down the spread of this process is its low reproducibility concerning the properties of parts. The low reproducibility is caused by the process complexity due to more than 50 process parameters influencing the part quality [3]. Understanding the process and the complex interactions between the different parameters is still part of an ongoing research [4,5].

Due to the high process complexity and low reproducibility, early research focused on investigating process monitoring techniques. Today, some machine manufacturers already offer monitoring techniques for industrial applications. Most of the monitoring techniques are based on monitoring the process emissions in the optical spectrum (plasma, reflected laser emission, thermal radiation). To collect these process signatures, sensors like cameras or diodes are placed off- or on-axis (coaxial to the laser beam) [6,7].

A novel approach, which is still in the research state and whose potential has not yet been assessed conclusively, is the acoustic monitoring of the L-PBF. Acoustic monitoring has already been applied in laser welding, where a distinction is made between air-borne acoustic

emission (ABAE) and structure-borne acoustic emission (SBAE) [8]. Since both approaches are known from monitoring laser welding processes, Section 2.1 summarizes, in total, 15 publications in order to provide an overview of the methods and approaches used. First publications on this topic emerged already in 1976. This is followed by a summary of the present work on acoustic monitoring regarding L-PBF in Section 2.2.

As of today, most process monitoring techniques available in industrial L-PBF machines provide feedback on process deviations [6]. However, such detecting of process deviations lacks the informative value of what may be experienced by the machine operator. He is unaware of the effects these deviations have on the function of the processed part and is thus limited in his actions. This work argues in favor of using part density as a measure of quality and as a more valuable feedback. Section 2.3, therefore, describes why this parameter is used and Section 3 describes the overall methodical approach. This includes the experimental setup to gather structure-borne acoustic emission (SBAE) data during the manufacturing process. For gathering the data, an exemplary process environment is used and is explained in Section 3.1. Section 3.2 describes the specimens used and the variation of process parameters in order to obtain parts of different density levels. One major challenge when analyzing acoustic data is the extraction of features from the raw acoustic signal. The short-time Fourier transform

(STFT) used for this work is argued and explained in Section 3.3. Archimedes' density measurements, giving results for 52 specimens, are described in Section 3.4. Section 3.5 concludes the methodical-approach part by describing the design of the artificial neural network (ANN) used. ANNs are implemented in this work by employing existing Python libraries (TensorFlow).

Section 4 is subdivided into two parts:

Section 4.1 determines whether it is possible to classify the resulting Archimedes' density level based on the acoustic data of one layer. To discuss the success, confusion matrix and F1-score are provided.

The robustness of the approach is compared in Section 4.2 by validating it using three different types of specimens that vary in their support geometry. This is of interest because the SBAE approach deals with acoustic waves that have to travel from the processed zone through the already finished part. In this case, dampening effects in complex geometries could reduce the performance of the monitoring technique. For this purpose, the robustness is discussed and evaluated in Section 4.2 by comparing the results of three different specimen types.

2. State of the art

Section 2.1 is a literature review of existing work on acoustic monitoring in laser welding. Section 2.2 summarizes the present work of acoustic monitoring in the L-PBF process. Furthermore, Section 2.3 provides a short discussion of quality definitions before arguing for the density measured using Archimedes' method.

2.1. Acoustic monitoring in laser welding and machine learning for data analysis

Regarding the aspect of monitoring laser welding, acoustic emissions (AE) have been widely investigated. First publications on this topic appeared about 40 years ago [9]. This literature research provides an overview of existing publications on acoustic process monitoring in laser welding. At the time of writing this article, there were four literature reviews concerning process monitoring of laser welding in general [10–13]. In total, 23 relevant papers are considered, 15 of which were published in scientific peer-reviewed articles that were included in this review. Table 1 summarizes the key findings which are explained in the following sections.

First of all, it is worth mentioning that all papers name two sources for acoustic emissions: evaporation dynamics and temperature gradients. Some of the works also propose formulas for the link between the acoustic source (in particular evaporation) and the acoustic pressure level [14–19].

Most of the papers investigate the influence of different process parameters on the acoustic signal. Commonly used parameters to determine the influence of the laser process on acoustic signals are scan speed and laser power. Some works also investigate the influence of focus variation on the acoustic signal. Only a few works focus on more quality-relevant parameters like penetration depth or gaps and misalignment failures and their influence on the acoustic signal.

In terms of signal processing, most of the papers analyze the signals in the frequency domain. Early works analyzed the intensity or signal pressure of the raw signal. Duley et al. [20] first transformed the signals into the frequency domain, which showed advantages for correlating acoustic signals with process characteristics. After 2000, either the fast Fourier transform (FFT) or wavelet functions have been used for all works, which underpins the advantage of analyzing acoustic signals in the frequency domain. The main advantages of signal analysis in the frequency domain are the better comparability and separability of different process conditions [20]. This is also valid when working with ANNs [19]. In addition, the filtering of noise is also mentioned to be more accessible in the frequency domain [21].

Moreover, investigations on automating signal analysis have increased in number over the years. Classification algorithms like artificial neural networks (ANN) [17,19,22] or pattern recognition [18,23] have been used to find links between the process and the acoustic signal. The approaches of these works are similar and, for providing a better insight, two of them are described in more detail.

Huang et al. [22] demonstrate that by using ANN, it is possible to predict the depth of the weld. The authors use two features forming the acoustic signal (sound pressure deviation and a frequency domain-based feature called band power) together with the set process parameters (laser power and welding speed) as an input for the ANN. Based on this input, the welding depth is predicted by the ANN. The resulting welding depth is determined with the help of views across sections.

Lee et al. show the full potential of data processing using ANNs [19]. In this paper, three different process conditions are distinguished (unsuccessful, successful, and over-welding, where thermal defects were apparent on the bottom of the specimen) and set by varying laser power and pulse duration resulting in 15 experiments. As input for the ANN, the amplitudes of three different frequency levels (100–200, 200–300, and $300-500$ kHz) are used. The ANN used is a multilayer perceptron (MLP). The ANN predicted the correct process condition classes with a precision of 88 %.

In the past years, other machine learning approaches like random forest models working with data sets similar to those used by Lee et al. have increased precision up to 95 % [24].

Table 1
Literature review for acoustic emissions in the laser beam melting process.

	Object of Investigation					Data Processing			Data Analysis		Type of AE		
	Scan parameter	Power	Focus	Defect	Penetration depth	Time domain	FFT	Wavelet	Manual	Auto	SBAE	ABAE	Max. freq. [kHz]
Saifi and Vahaviolos 1976 [9]				x		x			x		x		500
Duley and Mao 1994b [20]					x		x		x			x	10
Gu und Duley 1996a [23]			x		x		x			x		x	20
Nava-Rüdiger and Houlot 1997 [29]	x	x	x				x		x			x	20
Farson et al. 1997 [30]	x	x			x	x			x			x	20
Zeng et al. 2001 [16]				x				x		x		x	50
Luo et al. 2005 [17]				x			x	x	x			x	20
Bordatchev and Nikumb 2006 [18]			x			x	x		x			x	500
Huang and Kovacevic 2009a [31]	x	x			x		x		x			x	20
Khosroshahi et al. 2010 [32]		x					x		x			x	20
Huang and Kovacevic 2011 [22]	x	x			x		x			x		x	29
Lee et al. 2014 [19]	x	x		x			x			x	x		2000
Lee et al. 2015 [21]				x			x		x			x	40
Bastuck et al. 2016 [28]			x				x		x		x	x	1500
Shevchik et al. 2018b [24]		x					x	x		x	x	x	1850

In general, as mentioned in the introduction, there are two types of emissions produced in the process zone, one is called structure-borne acoustic emission (SBAE) and the other air-borne acoustic emission (ABAE). When comparing the findings from SBAE and ABAE, the following differences can be summarized.

For recording the ABAE, regular membrane microphones are used in most cases. For all SBAE approaches, piezoceramic transducers are used. ABAE is measured using up to 50 kHz, whereas SBAE is measured using up to 1000 kHz. This difference shows that SBAE has a broader frequency spectrum compared to ABAE. The broader frequency spectrum for SBAE is reasonable since there is higher damping of acoustic emissions in the air than in solid specimens [25].

The industrial application of SBAE in laser welding for quality control purposes is limited by the hardly reproducible coupling of the sensor to the workpiece [26]. This is a significant challenge for the laser welding process, since the sequence time in laser welding is only a few seconds before the workpiece changes, and the sensor has to be re-attached. It is essential for the analysis of SBAE that the sensor has a reproducible hardware connection to the workpiece. Hamann et al. [27] suggest to modify the sensor to meet this demand but do not evaluate it any further. The difficulties of attaching the sensor might be the reason why there is generally much more work done on the ABAE than on the SBAE.

In summary, the acoustic monitoring of ABAE and SBAE has shown good results for laser welding. ABAE has especially shown its advantages for evaluating process conditions correlating with plasma formation. SBAE has shown advantages in evaluating internal defects like the lack of penetration or porosity [28].

Most approaches are still at a laboratory research level only and are not industrially applicable. A reason for this could be the difficulty to interpret the signals and to handle the resulting significant amount of data.

Even though laser welding and L-PBF are two very similar processes, there are reasons why the approaches introduced laser welding need some adaption in order to monitor the L-PBF process. First of all, laser welding is a single-line process where only one vector is scanned. Compared to this, L-PBF works with hatching strategies which result in scanning several vectors for only one layer. This makes it clear that data processing and process result determination occur in different ways for L-PBF. Furthermore, the L-PBF process is slightly different from laser welding due to the different process morphology, and the desired process window is also different [33]. Nevertheless, the summarized publications provide relevant knowledge that has to be considered for the acoustic monitoring of L-PBF. It also underpins the potential of acoustic monitoring in laser processes.

2.2. Acoustic monitoring in the L-PBF process

Only very little research has so far been done on acoustic emission (AE) to monitor the L-PBF process. The following section will briefly introduce each available work. Table 2 summarizes the findings.

Rieder et al. [34] place a piezoelectric transducer for ultrasonic testing (UT) under a build platform. The UT unit transmits waves generated by the piezoelectric transducer and evaluates the recorded echo. Rieder et al. [34] briefly discuss the option of also using the transducer to monitor SBAE from the weld zone. During welding, SBAE signals were measured and plotted in a frequency spectrum. However, there was no further elaboration of the capabilities of this technique, since Rieder et al. [34] focused on the investigation of the potentials of UT during laser downtimes.

Two later works by Wasmer et al. [35] and Ye et al. [36] involved monitoring the air-borne acoustic emissions within the build chamber. Based on both experimental setups, further work by Ye et al. [37], Shevchik et al. [38], and Wasmer et al. [39] concentrates on data analysis. All of the publications mention that some form of ANN as well as signals in the frequency domain were used as input for the ANN. All

three publications aimed at distinguishing different classes of quality.

Ye et al. [39] determine quality according to the occurrence of balling, slight balling, regular process, slight overheating, and overheating. One significant restriction of this work is that all data were collected using single laser tracks. This means, only one layer of powder is molten by one laser scan line. The authors compare different setups of ANN (Multilayer Perceptron, Deep Believe Network, Support Vector Machine) and different inputs for the ANN (raw data, FFT, and FFT including denoising). A 95 % classification rate is reached with the Deep Believe Network and FFT, which is considered the best possible solution by the authors.

Shevchik et al. [37] and Wasmer et al. [38] use different scan speeds to obtain three different classes of density. Both publications used the same data set but performed different data analyses with different types of artificial neural networks. While Wasmer et al. [38] used wavelet-based features as input obtaining an overall accuracy between 79 % and 84 %, Shevchik et al. [37] used FFT-based features achieving an overall accuracy between 85 % and 89 %.

Another work by Wasmer et al. [40] also shows the connection between the welding condition and the SBAE. The authors introduce a test setup where acoustic data can be gathered in a high-speed x-ray computed tomography (CT). To collect acoustic data, a piezoelectric sensor is attached to the workpiece. Labeling (conduction welding, stable keyhole, unstable keyhole, spatter) of data is done according to the visual inspection of the CT images. The acoustic signal is transformed to Wavelets and then used for training. The results show that the welding condition can be matched to the acoustic signal. Therefore, a gradient boost method is used resulting in inaccurate values ranging between 74 % and 95 % depending on the class.

Besides these scientific works, the machine manufacturer, Renishaw, launched a system able to identify conspicuous events within the process with multiple integrated SBAE sensors, allowing for defect localization by means of triangulation. No scientific research on this system has been known so far. [41]

2.3. Process quality

In general, quality is defined by the customer and his satisfaction [43]. To satisfy a customer means to provide for the built part to meet the requirements of the customer; these in turn must be guaranteed by the process. Since the abilities to create new and better functions are the main reason (named by 70 % of a representative customer group) for using L-PBF [44], mechanical properties (e.g., stress behavior) likely have to be met by the produced part. Unfortunately, the mechanical properties (like tensile strength or fatigue behavior) are difficult to determine and go along with time-consuming destructive testing. However, to give a feedback nonetheless about the expected mechanical behavior, secondary quality parameters influencing the mechanical properties can be used as a measure of quality. This is a well-known process in the industry and is often done by tolerance management [45]. Unfortunately, there is not much information available on the tolerances used in the L-PBF process yet.

There is a lot of work available investigating the connection between process parameters, secondary quality parameters and the mechanical properties of the part, which help to understand the complex interaction between all these factors.

In general, the energy input is often altered in order to influence the process result. There are works showing, that high energy inputs support the formation of gas pores, while low energy inputs lead to fusion pores [6]. Reasons for having fusion pores can be traced back to a lack of energy, which is insufficient to form a constant melt pool. Compared to this, gas pores are typically formed when the energy input is too high and keyhole formation takes place in the process zone. In this situation, gas from evaporating alloys or process atmosphere gas can be trapped in a melt pool. Typically, gas pores are spherical and smaller in size than fusion pores [46–48]. Due to their shape and size fusion pores

Table 2
Literature review on acoustic emissions in the L-PBF process.

	Object of Investigation					Data Processing			Data Analysis		Type of AE		
	Type of Defect	Penetration depth	Focus	Scan parameter	Power	Time domain	FFT	Wavelet	Manual	Auto	SBAE	ABAE	Max freq. [kHz]
Rieder et al. 2016 [34]							x		x		x		–
Wasmer et al. 2017 [35]	x			x			x			x		x	1000
Ye et al. 2017 [36]				x	x				x				16
Wasmer et al. 2018 [38]	x			x				x		x		x	1000
Ye et al. 2018 [39]	x			x	x	x				x		x	16
Shevchik et al. 2018a [37]	x			x		x				x		x	1000
Wasmer et al. 2018 [40]	x	x						x		x	x		10,000
Gold und Spears 2018 [42]											x		–

have a much higher impact on the mechanical properties of the part.

Beside pores, the microstructure is a well-analyzed parameter in L-PBF. The microstructure is also highly influenced again by the energy input. Both crystallographic orientation and grain size can be controlled by altering the energy density. [49] In this context the melt pool size an overlap is highly influencing the microstructure [50]. Big melt pools from high energy input together with a high overlap lead to remelting of the martial which results in a bigger grain size [51]. In general it could be stated that defects like pores have a higher impact on the mechanical properties than microstructure [49].

Numerous further parameters are influencing the resulting mechanical properties (surface quality, residual stress, part orientation, etc.) [52–54] and the L-PBF process is a quite complex process resulting in a high variation and interaction of all of these factors. Future research will have to define the tolerances for these parameters to get reproducible products. For now, this work favors for density out of the named ones. The reason for this is that density is comparatively easy to evaluate and that it is often used as a measure for process success and benchmark within L-PBF [55]. Nevertheless, using only the density of a part as a measure of quality is a compromise and can only be the first starting point for monitoring the quality of L-PBF. To vary the density in the process, the energy density will be varied, which is a well-known approach in other works.

3. Methodical approach

This section explains the methodical approach of linking the acoustic signal with the density of a produced specimen. In order to reach this goal, Section 3.1 shows a suitable test setup for recording the structure-borne acoustic signal. After this, Section 3.2 explains the parameter selection and design of the specimens for recording data at different density and complexity levels. Section 3.3 focuses on the data processing of the raw acoustic signal. Reference measurements for

evaluating the density of each cube are performed and explained in Section 3.4 to obtain a data set for a supervised learning approach. An introduction to the ANN design itself is given in Section 3.5.

3.1. Experimental setup for recording structure-borne acoustic emissions

It is necessary to integrate a sensor as close as possible to the process zone in order to test the abilities of an SBAE approach in the L-PBF process. For this purpose, a test setup was built for this work and introduced by Eschner et al. [56]. Fig. 1 shows a view across sections of the test setup. The following section describes the setup and relevant components.

A continuous wave (CW) laser system provided by OR LASER with a wave length of 1064 nm and a peak power of 250 W, Gaussian beam profile and Raylase scan optics is used in the optical setup. The inert gas flow over the process zone is realized with the help of additive manufactured outlets and inlets (marked green in Fig. 1). A system provided by ULT AG filters particles from the inert gas and allows the inert gas to circulate via a controllable pump. An O_2 sensor (Microx Oxygen Analyzer) is integrated into the inert gas flow to measure the O_2 level.

In the build chamber (see sketch in Fig. 1), a simple recoater system wipes the powder from the reservoir to the built platform with a metal-supported rubber lip (marked dark red in Fig. 1). Stepper motors in the micro-stepping mode control the movement of all parts (a lip, coating, powder reservoir, built platform). All parts are placed in a sealed chamber, which guarantees inert process conditions. The whole system (motors, scanner, and laser) is controlled by LabView, which offers a high degree of freedom for adjusting the process parameters.

Regarding the material, 316 L (1.4404) is employed as it is a commonly used stainless steel alloy for L-PBF, but having a high demand for monitoring techniques, since it is more challenging to make post process CT scans due to the high material density. The powder is supplied in one batch by the company M4P. The powder is not reused in order to
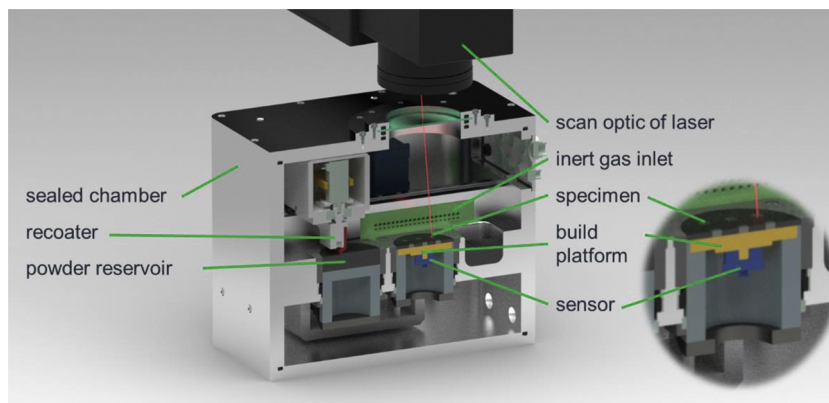

Fig. 1. Test bench setup for recording acoustic emissions in the L-PBF process.

Table 3
Process parameters and density for each specimen.

Porosity [%]	Plate	Laser-power [W]	Scan-speed [mm/s]	Hatching [mm]	Complexity Level	Class
−0.2	6	180	400	0.04	1	1
−0.1	6	180	200	0.04	1	1
0	2	180	200	0.04	2	1
0	3	180	200	0.05	3	1
0.1	1	180	200	0.05	2	1
0.1	1	180	400	0.05	2	1
0.2	1	130	200	0.05	2	1
0.2	5	180	200	0.05	1	1
0.4	1	130	400	0.05	2	1
0.4	2	130	200	0.04	2	1
0.4	3	130	200	0.05	3	1
0.5	2	180	400	0.04	2	1
0.5	4	180	200	0.04	3	1
0.5	6	130	200	0.04	1	1
0.7	3	180	400	0.05	3	1
0.7	4	180	400	0.04	3	1
0.7	5	130	200	0.05	1	1
0.9	3	130	400	0.05	3	1
1	1	180	1000	0.05	2	2
1	5	180	400	0.05	1	2
1.1	4	130	200	0.04	3	2
1.7	5	130	400	0.05	1	2
1.9	2	130	400	0.04	2	2
2.4	4	130	400	0.04	3	2
2.4	6	130	400	0.04	1	2
2.8	6	180	1000	0.04	1	2
3	3	180	1000	0.05	3	2
3.4	2	180	1000	0.04	2	2
3.6	5	180	1000	0.05	1	2
3.9	4	180	1000	0.04	3	2
4.9	2	130	1000	0.04	2	2
4.9	6	130	1000	0.04	1	2
5.2	1	130	1000	0.05	2	2
5.4	4	130	1000	0.04	3	2
5.4	5	130	1000	0.05	1	2
5.5	1	80	200	0.05	2	2
5.7	3	130	1000	0.05	3	3
6.2	3	80	200	0.05	3	3
6.3	5	80	200	0.05	1	3
6.7	2	80	200	0.04	2	3
6.9	4	80	200	0.04	3	3
7.4	6	80	200	0.04	1	3
12.4	6	80	400	0.04	1	3
12.7	4	80	400	0.04	3	3
13.6	1	80	400	0.05	2	3
14.1	3	80	400	0.05	3	3
14.7	5	80	400	0.05	1	3
15	2	80	400	0.04	2	3
25.6	4	80	1000	0.04	3	3
27.3	6	80	1000	0.04	1	3
29.2	2	80	1000	0.04	2	3
33.1	3	80	1000	0.05	3	3
34.3	5	80	1000	0.05	1	3
35.8	1	80	1000	0.05	2	3

Fig. 2. Built platform with nine specimens from top view [56].

purpose, the process parameters such as laser power (80, 130, 180 W), scan speed (200, 400, 1000 mm/s), and hatch distance (40, 50 μm) are altered. The parameter range is adjusted to the parameters employed in other works using 316 L to ensure processability [57–60]. The aim of this parameter selection is to generate specimens with high and low porosity levels. Therefore, a wide range of parameters are used.

Specimen have a cubical shape with an edge length of 5 mm. The described parameter selection results in a full factorial design of experiments with 18 cubes (see Table 3 for resulting parameter combinations). Cubes are placed in a 3 × 3 matrix shape on the built platform, as shown in Fig. 2.

In order to investigate the influence of part complexity, all 18 parameter combinations are built in three different levels of complexity (Fig. 3). Due to limitations of the software, only simple geometrical changes are possible to adjust complexity. Main goal of the complexity variation is to see if acoustic waves are influenced by the geometry. For this reason, a geometry simple enough to be printable with the test setup but complex enough to influence acoustic waves is chosen. The three resulting levels can be seen in Fig. 3. From the geometry, only the upper part of the specimens with an edge length of 5 mm (marked red in Fig. 3) is used for the following data analysis. This is necessary to guarantee the comparability of the acoustic signals in length and shape, which is essential for the used data processing approach. Also the following density measurement is only applied to the red marked part of the specimen. In total, 54 cubes (3 levels of laser power, 3 levels of scan speed, 2 levels of hatching distance, 3 level of complexity) are built, and the corresponding acoustic data is collected.

The generated parts are not representative of complex parts that can be printed with L-PBF. Nevertheless, these variations in geometry will help to understand whether SBAE monitoring only works for cubical specimens directly printed on the build plate or if the introduced geometrical cavities shield the acoustic signal in a way that they are not processable with the chosen approach.

3.3. Acoustic raw signal and feature extraction

The following sections explains the steps for data pre-processing starting from the raw signal gathered with the SBAE sensor.

By using a trigger generated by the LabView program, a single measurement file for each layer and each specimen is stored in the QASS Optimizer4D system. These files are then transferred from the QASS system to a personal computer after the production job is finished. On the computer, the data is decoded from the proprietary binary file format. Due to the findings presented in Section 2.1 regarding laser welding, where the analysis in the frequency domain showed clear advantages, now short time Fourier transform (STFT) is used for feature

avoid contamination from spatters and to ensure consistent powder parameters throughout all experiments.

Below the build platform (marked yellow in Fig. 1) of the process zone, an acoustic sensor (marked blue in Fig. 1) is mounted with a bolt. Glycerine is used as a coupling agent in order to guarantee a reproducible coupling. The sensor used is a massless piezoceramic sensor provided by QASS (model number: Q-WT-19 0232). A sampling rate of 4 MHz is used for the performed experiments. Preliminary tests showed that there are no relevant signals above 2 MHz, which also is in accordance with the findings mentioned in Section 2.1.

3.2. Design of specimen and parameter variation

Specimens with different density levels are built to find out if the monitoring system is capable of evaluating different densities. For this
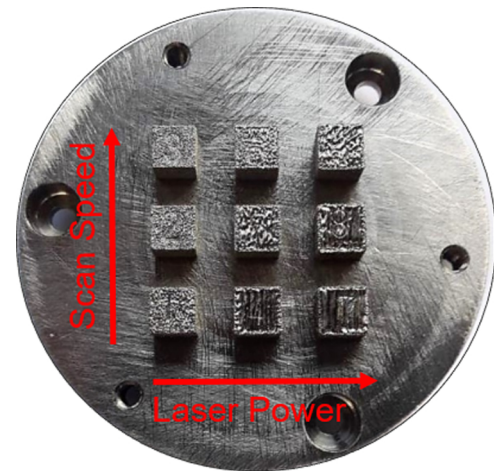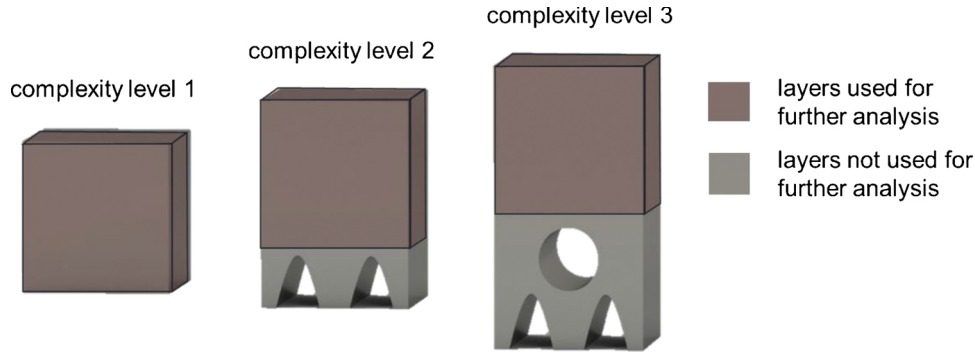
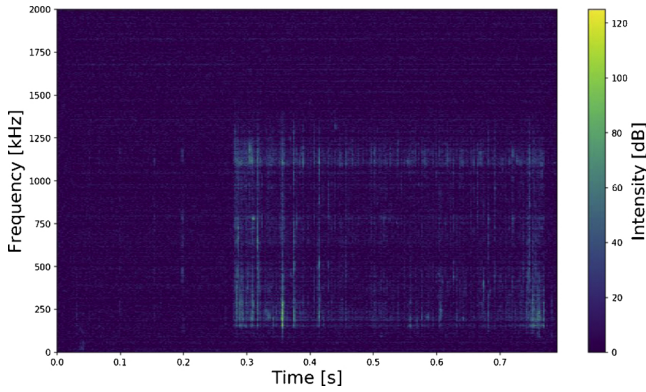**Fig. 3.** Specimen with different levels of complexity.

Fig. 4. Acoustic spectrogram for one layer of one specimen [56].

extraction. As a result, a spectrogram is obtained for each layer and each specimen. The obtained spectrograms are adjusted where needed to make sure that the spectrograms have the same number of samples. Shorter spectrograms are padded with the first ten samples of each measurement at the end.

Furthermore, to reduce noise, a difference mask generated out of the first 10 ms of each spectrogram is subtracted from the complete spectrogram. This difference mask represents the noise that is present without laser-material interaction. Noise is generated, for example, by the stepper motors or inert gas flow. Fig. 4 shows a spectrogram for one layer of one specimen after the STFT and subtraction of the difference mask.

From this spectrogram for each layer of each specimen, an input vector is derived containing the information of 12 million values of the spectrogram. For better convergence during the training phase, all input vectors are normalized. In total, 54 cubes are processed with each cube having 120 layers resulting in 6480 input vectors. These input vectors contain 12 million rows for the 12 million values of the spectrogram.

3.4. Reference measurements for determining process quality

In order to link the acoustic signal to the information of the expected part quality, the actual part quality has to be known. As pointed in Section 2.3, this work uses the density as a measure of part quality. Archimedes' density method is used to derive the density of all cubes. Two different approaches are used to calculate the density. One of them considers only the internal pores - Eq. (1), and the other one also considers surface-connected pores - Eq. (2).

In general, density is calculated by the mass of the body $\overline{m}_A$ over the volume. According to Archimedes, volume is calculated by buoyant force divided by the density of the fluid surrounding the specimen. For both equations, $\overline{m}_A$ is the measured weight of a cube surrounded by air with the density ρ_A. And $\overline{m}_F$ is the measured weight of a cube
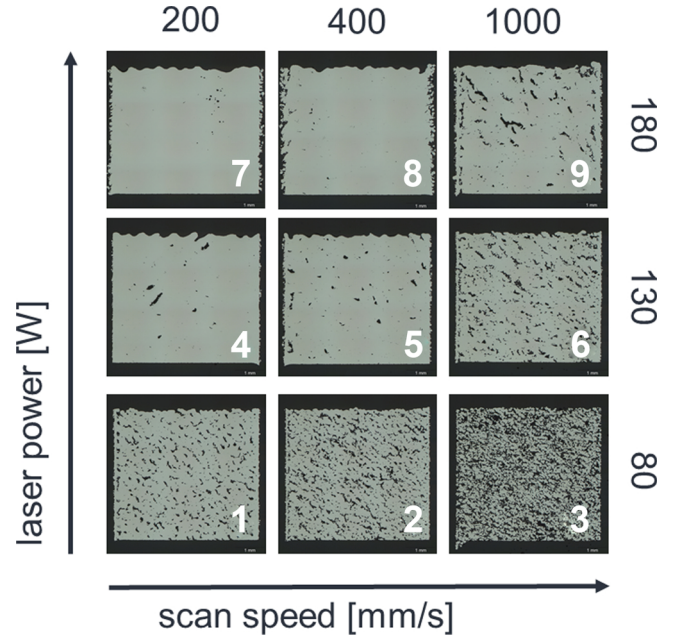

Fig. 5. Views across sections of plate number 5 of all nine cubes printed with the laser-power and scan-speed shown.

surrounded by the used measurement fluid which, in this case, is ethanol with the density ρ_F. To consider surface-connected pores, the cubes are impregnated with the measuring fluid, and the mass in the air is weighed which results in $\overline{m}_{AI}$ [61]. Eqs. (1) and (2) take into account the fact that the air buoyancy is acting as well on the specimen [55].

$$\rho^* = \frac{\overline{m}_A}{\overline{m}_A - \overline{m}_F}(\rho_F - \rho_A) + \rho_A \tag{1}$$

$$\rho^{**} = \frac{\overline{m}_A}{\overline{m}_{AI} - \overline{m}_F}(\rho_F - \rho_A) + \rho_A \tag{2}$$

In order to classify the porosity inside the cubes, Eq. (1) would be most suitable since lowest measurement uncertainties can be realized for this approach. However, it cannot be used for cubes printed with 80 W and 400 mm/s respectively 1000 mm/s on each plate with the lowest energy input (see Fig. 5 below red numbers 2 and 3). These cubes have mainly surface-connected pores, which leads to impregnation not only on the surface but throughout the complete cube volume. For this reason, Eq. (2), considering surface-connected pores, is used for the cube marked with red numbers 2 and 3. All measurements were performed five times by the same operator to determine the statistical variation of the measurement result.

Table 3 shows the results of Archimedes' density method. There are results indicating that there is a negative porosity. This is due to measurement uncertainty of the Archimedean density method.
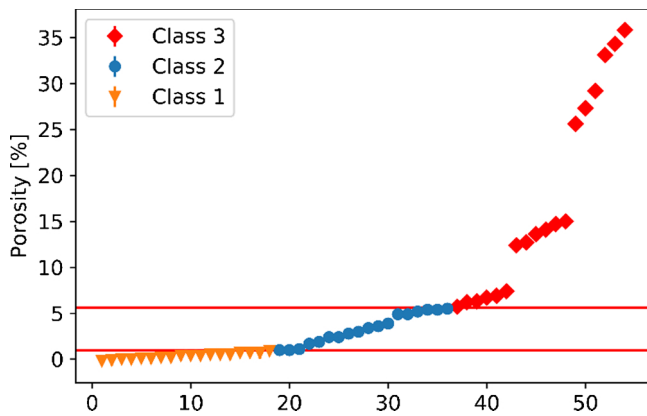
Fig. 6. Porosity in % for each cube and assignment to the three classes for each cube.
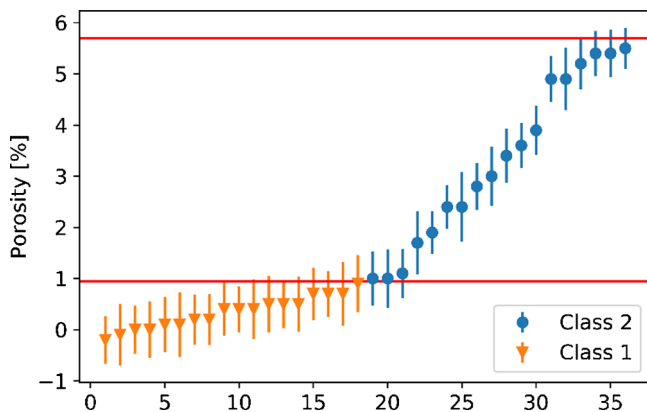

Fig. 7. Porosity in % for cubes of classes 1 and 2 with error bars from Archimedes' density method.

The relative density of the specimens varies between 65 % and 100.2 %. The reason for density to be over 100 % is caused by the measurement uncertainty. One reason for this is the not exactly known density of the measurement fluid. Since all cubes are measured with the same fluid it is just an offset and does not affect the further approach. Based on these results, three different density classes are derived. Each class has the same number of specimens. Fig. 6 illustrates the three classes. Class 1 has a density higher than 99 %. Class 2 has a density between 99 % and 94.3 %. Class-3 specimens have a density lower than 94.3 %. All class-3 cubes are built with the lowest laser power of 80 W.

Fig. 7 also includes error bars for the standard deviation of each measurement, but error bars are too small for being visible. In addition, Fig. 8 provides an overview of classes 1 and 2. In this figure, error bars are visible and show an overlap with the class boundaries.

3.5. Design of an artificial neural network

During the training process of the artificial neural network (ANN), each layer of a cube and its corresponding acoustic spectrogram (vector with 12 million values) represents one data set. The data sets are labeled according to the three classes derived from the part density described above in Section 3.4. In total, there are 2160 data sets available for each type of specimen and the respective complexity level. The data set is randomly split for all data sets into 70 % training and 30 % test data.

This work uses the multilayer perceptron (MLP) known as a typical ANN architecture. The MLP is one of the simpler neural networks available, as fewer hyperparameters are to be optimized. Therefore, it is preferred for the implementation in this work. The input layer consists of 12 million input neurons to be able to have the 12 million values of

the spectrogram as input. Two hidden layers follow the input layer with 64 and 32 neurons each, which is a bottleneck strategy. [62] This architecture performed best for the decided input compared to more hidden layers and more neurons shown in Eschner et al. [56].

The third and final layer consists of three output neurons for the three different density classes. Our approach uses the Sigmoid function as activation function for the individual neurons and Softmax for the output layer. Categorical cross entropy is used as loss function. The optimizer for backpropagation is ADAM.

Each training was set up for 100 epochs with early stopping based on validation loss after each epoch. This approach evaluates overfitting based on the development of accuracy and loss throughout the training epochs. [63] Training was done using a TensorFlow environment on an NVidia DGX station. The authors did not carry out any major adaptations to the provided algorithms from TensorFlow.

Precision, recall, and F1 score are derived from confusion matrices to measure and compare ANN performance. Precision defines the number of true positive classifications compared to all positive classifications ("What proportion of the classified data sets for class 1 is correctly classified as class 1?"[1]). In contrast, recall compares the true negative classifications to all real positives ("What proportion of data sets labeled as class 1 are identified by the algorithm to be class 1?"[2]). The F1 score combines precision and recall via Eq. (3):

$$F1 = \frac{2*(precision*recall)}{precision + recall} \tag{3}$$

Having three classes, an F1 score close to 0.33 is equivalent to guessing, and a F1 score of 1.0 would be an algorithm classifying all test data sets correctly. In this work, F1 score is preferred over accuracy to have a better measure for the incorrectly classified cases.

4. Results and discussion

This paper has two objectives: the first is to identify if it is possible to link the acoustic signal to a quality measure (Section 4.1). The second objective is to investigate if the geometry of the specimens influences the performance of structure-borne acoustic emission monitoring (Section 4.2).

4.1. Characterization of quality

The training discussed in this section considers all data sets of the 6480 layers for the 54 cubes to evaluate if a prediction of density is possible. As mentioned in Section 3.5, the input for the ANN is the spectrogram (as a vector with 12 million values) of each layer and each specimen. The output is the density class (labeled as class 1, class 2, and class 3), as described above in Section 3.4. Being a measure of the performance of the trained ANN, precision, recall, and F1 score are used as introduced in Section 3.5.

Table 4 shows the confusion matrix used for the test data classification. Table 5 shows the resulting performance parameters for each density class to classify the test data and the average values throughout all classes. For density class 1, performance is the best out of the three classes, precision is 86 %, and recall 91 %, which results in an F1 score of 89 %.

Class 2 is classified with the lowest performance, where all three performance parameters are below 80 %, but still higher than 73 %. The classification of the test data set for class 3 has a precision of 85 % and a recall of 83 %, which is again a little higher than the performance measures for class 2. Confusion matrix also shows that there are only a

---

[1] From: https://developers.google.com/machine-learning/crash-course/classification/precision-and-recall [22.08.2018]
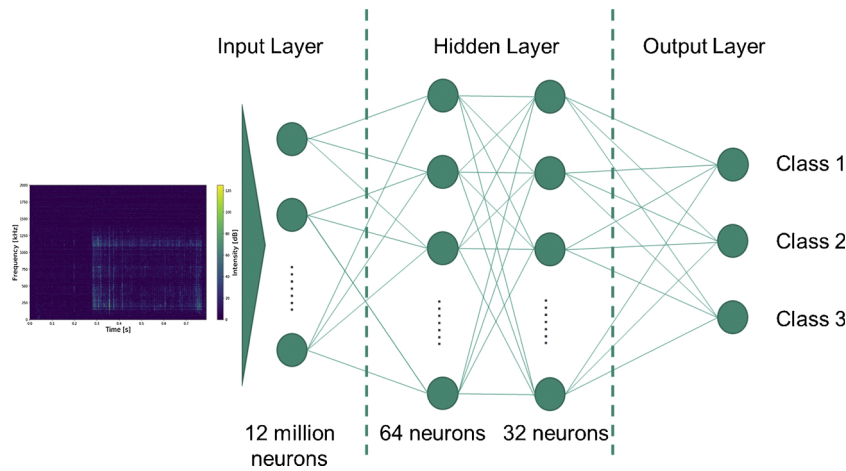[2] From: https://developers.google.com/machine-learning/crash-course/classification/precision-and-recall [22.08.2018]

Fig. 8. Shape of the used multilayer perceptron.

Table 4
Confusion matrix for the classification of density classes.

		Predicted class		
		1	2	3
	1	595	43	16
Actual class	**2**	87	454	80
	3	7	99	539

Table 5
Performance parameters used to classify density classes.

	Precision	Recall	F1 score
Class 1	0.86	0.91	0.89
Class 2	0.76	0.73	0.75
Class 3	0.85	0.84	0.84
Average	0.83	0.83	0.83

few data sets from class 1 classified as class 3 and vice versa.

The fact that the classification of class 1 is slightly better might be an indication that a good process resulting in a high part density has an acoustic spectrogram that can be more easily identified by the ANN. This finding goes along with the findings by Wasmer et al. [40] who found an algorithm identifying L-PBF- typical process conditions by using acoustic data.

Overall, the results prove that with the help of machine learning, it is possible to prove that there is a link between density and acoustic signals. The classification shows an average precision greater than 83 % with the described setup across all density classes. Performance is not as good as it is for some of the works reviewed in Section 2.1. Reasons for this might be the simplification of using one label over the whole cube, disregarding that there are layers with different density levels within one cube. Another reason is the uncertainty in making the classification labels on Archimedes' density measurement, which is indicated by the error bars in Fig. 7. There are cubes classified in class 1 even though there is a statistical probability that this cube actually has to be class 2. Nevertheless, these results clearly show the potential of characterizing density based on SBAE from the process.

4.2. Transfer to more complex test geometries

After the ANN has successfully learned to link part density and acoustic signals, the focus of this section is now to determine if the geometry complexity of the specimen influences the performance.

Table 6
Performance parameters for the classification of density classes with models trained for a certain complexity level.

		F1 score average		
Complexity level		1	2	3
	1	0.88	0.69	0.61
Model	2	0.66	0.86	0.65
	3	0.55	0.65	0.85

Therefore, three different ANN models for each complexity level are trained in the same way as in Section 4.1. Table 6 shows the average F1 score for each model used on the corresponding test data set. Table 7 provides the underlying confusion matrixes.

The dataset for training of each model is smaller compared to data sets used in Section 4.1 and gives reason to expect worse performance parameters. Overall, the performance parameters for each model within the trained complexity level is even slightly better than the performance of the model trained by using the whole data set in 4.1. The average F1 score for all three complexity levels is between 85 % and 88 %.

Comparing the performance values with the complexity levels, F1 score is 88 % for the lowest complexity (level 1), 86 % for medium complexity (level 2), and 85 % for the highest complexity (level 3). These results show that performance is only slightly worsening as complexity increases. As shown in Eschner et al. [56], these variations are within the uncertainty when training an ANN model and are seen as not significant. Based on these results, it is possible to assume that the approach also works for more complex geometries, as long as the model is trained for each geometry.

To further analyze the potential of using one model for different geometries, the trained model of each complexity level is used by applying it to the dataset of other complexity levels. With this procedure, it is possible to get an idea of the robustness the trained models offer when applying them to unknown geometries

Tables 6 and 7 show the resulting performance scores for the different models applied to the data sets they are not trained for. At this point, the performance values show that the performance is clearly declining. Looking at model 1 (trained on the basis of the data set for the lowest complexity), the F1 score drops to 61 % for the highest complexity. And the model trained on the basis of the highest complexity level (model 3) has a F1 score that is as low as 56 %. This result might also explain why the model trained in Section 4.1 scores a little lower than the ones trained for each complexity level individually. The authors assume that the established models work best when applied to

Table 7
Confusion matrixes for the classification of density classes with models trained for a certain complexity level.

			Complexity level 1				Complexity level 2				Complexity level 3		
				Pred.				**Pred.**				**Pred.**	
			1	**2**	**3**		**1**	**2**	**3**		**1**	**2**	**3**
Model	1	**Actual 1**	173	8	3	**Actual 1**	142	69	39	**Actual 1**	123	85	22
		2	6	209	23	**2**	4	153	54	**2**	45	125	6
		3	3	36	179	**3**	3	33	143	**3**	12	80	142
				Pred.				**Pred.**				**Pred.**	
			1	**2**	**3**		**1**	**2**	**3**		**1**	**2**	**3**
	2	**Actual 1**	179	0	5	**Actual 1**	225	14	11	**Actual 1**	209	10	11
		2	72	122	44	**2**	9	175	27	**2**	77	82	17
		3	23	67	128	**3**	10	16	153	**3**	35	67	132
				Pred.				**Pred.**				**Pred.**	
			1	**2**	**3**		**1**	**2**	**3**		**1**	**2**	**3**
	3	**Actual 1**	147	31	6	**Actual 1**	231	6	13	**Actual 1**	204	7	19
		2	90	55	93	**2**	49	60	102	**2**	8	146	22
		3	33	10	175	**3**	28	5	146	**3**	9	32	193

the geometry they were actually trained for. Further works need to find a way to analyze and process data so that the approach becomes robust to geometric variations.

5. Summary and future work

This publication provided an overview of the systems used for monitoring acoustic emission (AE) in laser processes. The literature review underpinned the existing high potential in the use of structure-borne acoustic emission (SBAE) for monitoring laser processes. Section 3.1 introduced a test setup and approach to investigate the potential of using SBAE to monitor the L-PBF process.

Results in Section 4 underpin the ability to use SBAE for process monitoring. Section 4.1 showed the ability to classify Archimedes' part density by analyzing the acoustic signal in a frequency domain with the help of an ANN. For the ANN training, a data set containing 54 specimens with different density levels was used. F1 scores up to 88 % were found, which indicates a connection of acoustic signal and part density as a measure of quality.

Nevertheless, the results in Section 4.2 also showed that more work is needed to make the approach transferable to other geometries and new data sets. Therefore, different measures are in focus:

a) Further types of feature extraction have to be tested. As Wasmer et. al. [38] and Shevchik et. al [24]. have shown, wavelet transformation works for analyzing these types of acoustic data. Further feature extraction of statistic features out of the spectrograms should also be tested in order to reduce the data set size.
b) In this work, only a simple ANN or rather an MLP is used. Future work should try to work with more complex types of ANN, e.g. a convolutional neural network (CNN). These types of ANN are known for performing better and being more robust but also need more data.
c) The goal of future work should also be to identify a single event of defect formation and the corresponding characteristic acoustic emission. With this, it is very likely to obtain an approach that is more robust to geometric variations. Other reference measuring methods such as computed tomography have to be qualified to match single defects like matching one specific pore to a certain acoustic signal.
d) Since this is a data-driven approach, more data will help to make it more robust. Especially more data on different geometries should be collected.

It would also be essential to use different and more realistic mechanisms which are known for causing defects in order to make the monitoring technique more robust. Right now, the state of the art for testing process monitoring techniques is to vary process parameters such as laser power or scan speed, since these parameters are easy to adjust. The risk at this point is that the ANN learns to detect the change of these parameters and not the defect formation itself. Further research has thus to focus on finding other ways of varying the density of specimens that are more similar to the defects occurring in an industrial application.

With the current hardware, the setup time to make a spectrogram for one layer is about 1 min on a desktop computer. Training of an ANN takes approximately 4 h on a NVidia DGX station. Moreover, the classification of a given spectrogram takes about 2 min, which is mainly limited by the mass storage speed of the used computer. All the codes and hardware are not yet optimized for fast calculation and in-process classification. Future activities on the subject will find a way to reduce the time from raw signal to classification with a given ANN.

Future works will also focus on the combination of the SBAE monitoring techniques with other monitoring techniques like ABAE or optical ones. It is very likely that these techniques have their advantages and work much better when combined.

Conflict of interests

The authors declare the following financial interests/personal relationships which may be considered as potential competing interests:

References

[1] T. Wohlers, T. Caffrey, R.I. Campbell, O. Diegel, J. Kowen, Wohlers Report 2018: 3D

Printing and Additive Manufacturing State of the Industry; Annual Worldwide Progress Report, Wohlers Associates, 2018.

[2] A. Gebhardt, J.-S. Hötter, Additive Manufacturing: 3D Printing for Prototyping and Manufacturing, Hanser Publishers; Hanser Publications, Munich, Cincinnati, 2016.

[3] T.G. Spears, S.A. Gold, In-process sensing in selective laser melting (SLM) additive manufacturing, Integr Mater Manuf Innov 5 (2016) 683, https://doi.org/10.1186/s40192-016-0045-4.

[4] A.M. Khorasani, I. Gibson, A. Ghasemi, A. Ghaderi, A comprehensive study on variability of relative density in selective laser melting of Ti-6Al-4V, Virtual Phys. Prototyp. 14 (2019) 349–359, https://doi.org/10.1080/17452759.2019.1614198.

[5] W.H. Yu, S.L. Sing, C.K. Chua, C.N. Kuo, X.L. Tian, Particle-reinforced metal matrix nanocomposites fabricated by selective laser melting: a state of the art review, Prog. Mater. Sci. 104 (2019) 330–379, https://doi.org/10.1016/j.pmatsci.2019.04.006.

[6] S.K. Everton, M. Hirsch, P. Stravroulakis, R.K. Leach, A.T. Clare, Review of in-situ process monitoring and in-situ metrology for metal additive manufacturing, Mater. Des. 95 (2016) 431–445, https://doi.org/10.1016/j.matdes.2016.01.099.

[7] M. Grasso, B.M. Colosimo, Process defects and in situ monitoring methods in metal powder bed fusion: a review, Meas. Sci. Technol. 28 (2017) 44005.

[8] A. Ali, D. Farson, Statistical classification of spectral data for laser weld quality monitoring, Int. J. Mach. Tools Manuf. 124 (2002) 323, https://doi.org/10.1115/1.1455028.

[9] M. Saifi, S. Vahaviolos, Laser spot welding and real-time evaluation, IEEE J. Quantum Electron. 12 (1976) 129–136, https://doi.org/10.1109/JQE.1976.1069104.

[10] J. Shao, Y. Yan, Review of techniques for on-line monitoring and inspection of laser welding, J. Phys. Conf. Ser. 15 (2005) 101–107, https://doi.org/10.1088/1742-6596/15/1/017.

[11] A. Sun, E. Kannatey-Asibu, M. Gartner, Sensor systems for real-time monitoring of laser weld quality, J. Laser Appl. 11 (1999) 153–168, https://doi.org/10.2351/1.521893.

[12] T. Purtonen, A. Kalliosaari, A. Salminen, Monitoring and adaptive control of laser processes, Phys. Procedia 56 (2014) 1218–1231, https://doi.org/10.1016/j.phpro.2014.08.038.

[13] J. Stavridis, A. Papacharalampopoulos, P. Stavropoulos, Quality assessment in laser welding: a critical review, Int J Adv Manuf Technol 94 (2018) 1825–1847, https://doi.org/10.1007/s00170-017-0461-4.

[14] W.W. Duley, Y.L. Mao, The effect of surface condition on acoustic emission during welding of aluminium with CO 2 laser radiation, J. Phys. D Appl. Phys. 27 (1994) 1379–1383, https://doi.org/10.1088/0022-3727/27/7/007.

[15] H. Gu, W.W. Duley, A statistical approach to acoustic monitoring of laser welding, J. Phys. D Appl. Phys. 29 (1996) 556.

[16] H. Zeng, Z. Zhou, Y. Chen, H. Luo, L. Hu, Wavelet analysis of acoustic emission signals and quality control in laser welding, J. Laser Appl. 13 (2001) 167–173, https://doi.org/10.2351/1.1386799.

[17] H. Luo, H. Zeng, L. Hu, X. Hu, Z. Zhou, Application of artificial neural network in laser welding defect diagnosis, J. Mater. Process. Technol. 170 (2005) 403–411, https://doi.org/10.1016/j.jmatprotec.2005.06.008.

[18] E.V. Bordatchev, S.K. Nikumb, Effect of focus position on informational properties of acoustic emission generated by laser–material interactions, Appl. Surf. Sci. 253 (2006) 1122–1129, https://doi.org/10.1016/j.apsusc.2006.01.047.

[19] S. Lee, S. Ahn, C. Park, Analysis of acoustic emission signals during laser spot welding of SS304 stainless steel, J. of Materi Eng and Perform 23 (2014) 700–707, https://doi.org/10.1007/s11665-013-0791-9.

[20] W.W. Duley, Y.L. Mao, The effect of surface condition on acoustic emission during welding of aluminium with CO2 laser radiation, J. Phys. D Appl. Phys. 27 (1994) 1379.

[21] C.-J. Lee, J.-D. Kim, Y.-C. Kim, Study on monitoring of plasma emission signal in lap welding of Zn coated steel sheet using CO2 laser, Int. J. Precis. Eng. Manuf. Technol. 16 (2015) 495–500, https://doi.org/10.1007/s12541-015-0067-4.

[22] W. Huang, R. Kovacevic, A neural network and multiple regression method for the characterization of the depth of weld penetration in laser welding based on acoustic signatures, J. Intell. Manuf. 22 (2011) 131–143, https://doi.org/10.1007/s10845-009-0267-9.

[23] H. Gu, W.W. Duley, A statistical approach to acoustic monitoring of laser welding, J. Phys. D Appl. Phys. 29 (1996) 556–560, https://doi.org/10.1088/0022-3727/29/3/011.

[24] S. Shevchik, T. Le-Quang, B. Meylan, K. Wasmer, Acoustic emission for in situ monitoring of laser processing, 33rd European Conference on Acoustic Emission Testing (EWGAE) 33 (2018).

[25] V. Deutsch, M. Platte, M. Vogt, Ultraschallprüfung: Grundlagen Und Industrielle Anwendungen, Springer-Verlag, 2013.

[26] W. Huang, R. Kovacevic, Acoustic monitoring of weld penetration during laser welding of high strength steels, International Congress on Applications of Lasers & Electro-Optics, Laser Institute of America, November 2–5 (2009) 630–637.

[27] C. Hamann, H.-G. Rosen, B. LaBiger, Acoustic emission and its application to laser spot welding, in: M. Gaillard, A. Quenzer (Eds.), High Power Lasers and Laser Machining Technology, SPIE, 1989, p. 275.

[28] M. Bastuck, H.-G. Herrmann, B. WOLTER, D. BÖTTGER, P.-C. ZINN, Acoustic inline process monitoring for laser welding applications, World Conference on Nondestructive Testing (19): WCNDT 2016 (2016).

[29] E. Nava-Rüdiger, M. Houlot, Integration of real time quality control systems in a welding process, J. Laser Appl. 9 (1997) 95–102, https://doi.org/10.2351/1.4745449.

[30] D. Farson, Y. Sang, A. Ali, Relationship between airborne acoustic and optical emissions during laser welding, J. Laser Appl. 9 (1997) 87–94, https://doi.org/10.2351/1.4745448.

[31] W. Huang, R. Kovacevic, Feasibility study of using acoustic signals for online monitoring of the depth of weld in the laser welding of high-strength steels, Journal of Engineering Manufacture 223 (2009) 343–361, https://doi.org/10.1243/09544054JEM1320.

[32] M.E. Khosroshahi, F.A. pour, M. Hadavi, M. Mahmoodi, In situ monitoring the pulse CO2 laser interaction with 316-L stainless steel using acoustical signals and plasma analysis, Appl. Surf. Sci. 256 (2010) 7421–7427, https://doi.org/10.1016/j.apsusc.2010.05.083.

[33] R. Cunningham, C. Zhao, N. Parab, C. Kantzos, J. Pauza, K. Fezzaa, T. Sun, A.D. Rollett, Keyhole threshold and morphology in laser melting revealed by ultrahigh-speed x-ray imaging, Science 363 (2019) 849–852, https://doi.org/10.1126/science.aav4687.

[34] H. Rieder, M. Spies, J. Bamberg, B. Henkel, On- and Offline Ultrasonic Characterization of Components Built by SLM Additive Manufacturing, AIP Publishing LLC, 2016, p. 130002.

[35] K. Wasmer, C. Kenel, C. Leinenbach, S.A. Shevchik, In situ quality monitoring in AM using Acoustic Emission: a machine learning approach, Materials Science and Technology (MS&T17) (2017) 386–388, https://doi.org/10.7449/2017/MST_2017_386_388.

[36] D. Ye, Z. Yingjie, Z. Kunpeng, H. Geok-Soon, Y. Jerry, Characterization of Acoustic Signals During a Direct Metal Laser Sintering Process, (2017), pp. 1315–1320.

[37] S.A. Shevchik, C. Kenel, C. Leinenbach, K. Wasmer, Acoustic emission for in situ quality monitoring in additive manufacturing using spectral convolutional neural networks, Addit. Manuf. 21 (2018) 598–604, https://doi.org/10.1016/j.addma.2017.11.012.

[38] K. Wasmer, C. Kenel, C. Leinenbach, S.A. Shevchik, In situ and Real-time monitoring of powder-bed AM by combining acoustic emission and artificial intelligence, in: M. Meboldt, C. Klahn (Eds.), Industrializing Additive Manufacturing - Proceedings of Additive Manufacturing in Products and Applications - AMPA2017, Springer International Publishing, Cham, 2018, pp. 200–209.

[39] D. Ye, G.S. Hong, Y. Zhang, K. Zhu, J.Y.H. Fuh, Defect detection in selective laser melting technology by acoustic signals with deep belief networks, Int J Adv Manuf Technol 96 (2018) 2791–2801, https://doi.org/10.1007/s00170-018-1728-0.

[40] K. Wasmer, T. Le-Quang, B. Meylan, F. Vakili-Farahani, M.P. Olbinado, A. Rack, S.A. Shevchik, Laser processing quality monitoring by combining acoustic emission and machine learning: a high-speed X-ray imaging approach, Procedia Cirp 74 (2018) 654–658, https://doi.org/10.1016/j.procir.2018.08.054.

[41] Chris Pockett, Renishaw Launches New Software to Improve Additive Manufacturing (AM) Quality, (2019).

[42] S.A. Gold, T.G. Spears, Acoustic monitoring method for additive manufacturing processes, Google Patents, 2018.

[43] R. Reed, D.J. Lemak, N.P. Mero, Total quality management and sustainable competitive advantage, J. Qual. Manag. 5 (2000) 5–26, https://doi.org/10.1016/S1084-8568(00)00010-9.

[44] G. Lanza, R. Kopf, M. Zaiß, N. Stricker, N. Eschner, A. Jacob, S. Yang, A. Schönle, L. Webersinke, L. Wirsig, Laser-Strahlschmelzen - Technologie Mit Zukunftspotenzial: Ein Handlungsleitfaden, 2017th ed., KIT, Karlsruhe Institut für Technologie, wbk Institut für Produktionstechnik, Karlsruhe, 2017.

[45] A. Etienne, J.-Y. Dantan, J. Qureshi, A. Siadat, Variation management by functional tolerance allocation and manufacturing process selection, Int. J. Interact. Des. Manuf. 2 (2008) 207–218, https://doi.org/10.1007/s12008-008-0055-3.

[46] H. Gong, K. Rafi, H. Gu, T. Starr, B. Stucker, Analysis of defect generation in Ti–6Al–4V parts made using powder bed fusion additive manufacturing processes, Addit. Manuf. 1–4 (2014) 87–98, https://doi.org/10.1016/j.addma.2014.08.002.

[47] W.E. King, H.D. Barth, V.M. Castillo, G.F. Gallegos, J.W. Gibbs, D.E. Hahn, C. Kamath, A.M. Rubenchik, Observation of keyhole-mode laser melting in laser powder-bed fusion additive manufacturing, J. Mater. Process. Technol. 214 (2014) 2915–2925, https://doi.org/10.1016/j.jmatprotec.2014.06.005.

[48] G. Kasperovich, J. Haubrich, J. Gussone, G. Requena, Correlation between porosity and processing parameters in TiAl6V4 produced by selective laser melting, Mater. Des. 105 (2016) 160–170, https://doi.org/10.1016/j.matdes.2016.05.070.

[49] A. Leicht, M. Rashidi, U. Klement, E. Hryha, Effect of process parameters on the microstructure, tensile strength and productivity of 316L parts produced by laser powder bed fusion, Mater. Charact. 159 (2020) 110016, , https://doi.org/10.1016/j.matchar.2019.110016.

[50] C.N. Kuo, C.K. Chua, P.C. Peng, Y.W. Chen, S.L. Sing, S. Huang, Y.L. Su, Microstructure evolution and mechanical property response via 3D printing parameter development of Al–Sc alloy, Virtual Phys. Prototyp. 15 (2020) 120–129, https://doi.org/10.1080/17452759.2019.1698967.

[51] S.K. Nayak, S.K. Mishra, C.P. Paul, A.N. Jinoop, K.S. Bindra, Effect of energy density on laser powder bed fusion built single tracks and thin wall structures with 100 μm preplaced powder layer thickness, Opt. Laser Technol. 125 (2020) 106016, , https://doi.org/10.1016/j.optlastec.2019.106016.

[52] Y.J. Liu, S.J. Li, H.L. Wang, W.T. Hou, Y.L. Hao, R. Yang, T.B. Sercombe, L.C. Zhang, Microstructure, defects and mechanical behavior of beta-type titanium porous structures manufactured by electron beam melting and selective laser melting, Acta Mater. 113 (2016) 56–67, https://doi.org/10.1016/j.actamat.2016.04.029.

[53] E. Beevers, A.D. Brandão, J. Gumpinger, M. Gschweitl, C. Seyfert, P. Hofbauer, T. Rohr, T. Ghidini, Fatigue properties and material characteristics of additively manufactured AlSi10Mg – effect of the contour parameter on the microstructure, density, residual stress, roughness and mechanical properties, Int. J. Fatigue 117 (2018) 148–162, https://doi.org/10.1016/j.ijfatigue.2018.08.023.

[54] A. Yadollahi, N. Shamsaei, Additive manufacturing of fatigue resistant materials: challenges and opportunities, Int. J. Fatigue 98 (2017) 14–31, https://doi.org/10.1016/j.ijfatigue.2017.01.001.

[55] A.B. Spierings, M. Schneider, R. Eggenberger, Comparison of density measurement

techniques for additive manufactured metallic parts, Rapid Prototyp. J. 17 (2011) 380–386, https://doi.org/10.1108/13552541111156504.

[56] Development of an Acoustic Process Monitoring System for the Selective Laser Melting (SLM), in: N. Eschner, L. Weiser, B. Häfner, G. Lanza (Eds.), SFF Symposium, Austin, Texas, 2018.

[57] A.B. Spierings, G. Levy, Comparison of density of stainless steel 316L parts produced with selective laser melting using different powder grades, Proceedings of the Annual International Solid Freeform Fabrication Symposium, Austin, TX, 2009, pp. 342–353.

[58] A. Laohaprapanon, P. Jeamwatthanachai, M. Wongcumchang, N. Chantarapanich, S. Chantaweroad, K. Sitthiseripratip, S. Wisutmethangoon, Optimal scanning condition of selective laser melting processing with stainless steel 316L powder, in: L. Guiping (Ed.), Material and Manufacturing Technology II: Selected, Peer Reviewed Papers from the 2011 2nd International Conference on Material and Manufacturing Technology (ICMMT 2011), July 8-11, 2011, Xiamen, China, Trans Tech Publ, Durnten-Zurich, 2012, pp. 816–820.

[59] I. Yadroitsev, I. Yadroitsava, Evaluation of residual stress in stainless steel 316L and Ti6Al4V samples produced by selective laser melting, Virtual Phys. Prototyp. 10 (2015) 67–76, https://doi.org/10.1080/17452759.2015.1026045.

[60] K. Saeidi, J. Olsen, Z. Shen, Scaled down microstructure hierarchy and local heterogeneity in laser melted 316L stainless steel, Mater. Charact. (2016).

[61] S. Bai, N. Perevoshchikova, Y. Sha, X. Wu, The effects of selective laser melting process parameters on relative density of the AlSi10Mg parts and suitable procedures of the archimedes method, Appl. Sci. 9 (2019) 583, https://doi.org/10.3390/app9030583.

[62] D. Yu, M.L. Seltzer, Improved Bottleneck Features Using Pretrained Deep Neural Networks, in: Twelfth Annual Conference of the International Speech Communication Association, (2011).

[63] A. Gulli, S. Pal, Deep Learning With Keras, Packt Publishing, Birmingham, 2017.